Research Article | Vol. 7, No. 9 | 1 Sep 2016 | BIOMEDICAL OPTICS EXPRESS 3531
Biomedical Optics EXPRESS

Handheld nonlinear microscope system comprising a 2 MHz repetition rate, mode-locked Yb-fiber laser for *in vivo* biomedical imaging

ÁDÁM KROLOPP,[1,2] ATTILA CSÁKÁNYI,[1] DÓRA HALUSZKA,[1,3] DÁNIEL CSÁTI,[2] LAJOS VASS,[2] ATTILA KOLONICS,[1,2] NORBERT WIKONKÁL,[3] AND RÓBERT SZIPŐCS[1,2,*]

[1]*Wigner RCP, Institute for Solid State Physics and Optics, P.O. Box 49, H-1525 Budapest, Hungary*
[2]*R & D Ultrafast Lasers Ltd, P.O. Box 622, H-1539 Budapest, Hungary*
[3]*Department of Dermatology, Venereology and Dermatooncology, Semmelweis University, H-1085 Budapest, Hungary*
[*]*r.szipocs@szipocs.com*
https://www.szipocs.com

Abstract: A novel, Yb-fiber laser based, handheld 2PEF/SHG microscope imaging system is introduced. It is suitable for *in vivo* imaging of murine skin at an average power level as low as 5 mW at 200 kHz sampling rate. Amplified and compressed laser pulses having a spectral bandwidth of 8 to 12 nm at around 1030 nm excite the biological samples at a ~1.89 MHz repetition rate, which explains how the high quality two-photon excitation fluorescence (2PEF) and second harmonic generation (SHG) images are obtained at the average power level of a laser pointer. The scanning, imaging and detection head, which comprises a conventional microscope objective for beam focusing, has a physical length of ~180 mm owing to the custom designed imaging telescope system between the laser scanner mirrors and the entrance aperture of the microscope objective. Operation of the all-fiber, all-normal dispersion Yb-fiber ring laser oscillator is electronically controlled by a two-channel polarization controller for Q-switching free mode-locked operation. The whole nonlinear microscope imaging system has the main advantages of the low price of the fs laser applied, fiber optics flexibility, a relatively small, light-weight scanning and detection head, and a very low risk of thermal or photochemical damage of the skin samples.

©2016 Optical Society of America

OCIS codes: (140.7090) Ultrafast lasers; (170.1870) Dermatology; (180.4315) Nonlinear microscopy.

References and links

1. M. Klemp, M. C. Meinke, M. Weinigel, H. J. Röwert-Huber, K. König, M. Ulrich, J. Lademann, and M. E. Darvin, "Comparison of morphologic criteria for actinic keratosis and squamous cell carcinoma using in vivo multiphoton tomography," Exp. Dermatol. **25**(3), 218–222 (2016).
2. M. Weinigel, H. G. Breunig, A. Uchugonova, and K. König, "Multipurpose nonlinear optical imaging system for in vivo and ex vivo multimodal histology," J. Med. Imaging (Bellingham) **2**(1), 016003 (2015).
3. M. Balu, C. B. Zachary, R. M. Harris, T. B. Krasieva, K. König, B. J. Tromberg, and K. M. Kelly, "In vivo multiphoton microscopy of basal cell carcinoma," JAMA Dermatol. **151**(10), 1068–1074 (2015).
4. M. Balu, K. M. Kelly, C. B. Zachary, R. M. Harris, T. B. Krasieva, K. König, A. J. Durkin, and B. J. Tromberg, "Distinguishing between benign and malignant melanocytic nevi by in vivo multiphoton microscopy," Cancer Res. **74**(10), 2688–2697 (2014).
5. M. Balu, A. Mazhar, C. K. Hayakawa, R. Mittal, T. B. Krasieva, K. König, V. Venugopalan, and B. J. Tromberg, "In vivo multiphoton NADH fluorescence reveals depth-dependent keratinocyte metabolism in human skin," Biophys. J. **104**(1), 258–267 (2013).
6. E. J. Mayer, J. Möbius, A. Euteneuer, W. W. Rühle, and R. Szipőcs, "Ultrabroadband chirped mirrors for femtosecond lasers," Opt. Lett. **22**(8), 528–530 (1997).
7. K. Kieu and F. W. Wise, "All-fiber normal-dispersion femtosecond laser," Opt. Express **16**(15), 11453–11458 (2008).
8. J. Fekete, A. Cserteg, and R. Szipőcs, "All-fiber, all-normal dispersion ytterbium ring oscillator," Laser Phys. Lett. **6**(1), 49–53 (2009).

#269667 http://dx.doi.org/10.1364/BOE.7.003531
Journal © 2016 Received 1 Jul 2016; revised 11 Aug 2016; accepted 16 Aug 2016; published 19 Aug 2016

Biomedical Optics EXPRESS

9. B. G. Saar, R. S. Johnston, C. W. Freudiger, X. S. Xie, and E. J. Seibel, "Coherent Raman scanning fiber endoscopy," Opt. Lett. **36**(13), 2396–2398 (2011).
10. D. Herrmann, J. Eastman, Ch. Alessi-Fox, and N. Boger, "Non-invasive in-vivo imaging of mechanoreceptors in human skin using confocal microscopy," U.S. Patent 11/878,638 (2007).
11. P. Antal and R. Szipőcs, "Tunable, low-repetition-rate, cost-efficient femtosecond Ti:sapphire laser for nonlinear microscopy," Appl. Phys. B **107**(1), 17–22 (2012).
12. M. Baumgartl, M. Chemnitz, C. Jauregui, T. Meyer, B. Dietzek, J. Popp, J. Limpert, and A. Tünnermann, "All-fiber laser source for CARS microscopy based on fiber optical parametric frequency conversion," Opt. Express **20**(4), 4484–4493 (2012).
13. D. Haluszka, K. Lőrincz, R. Szipőcs, N. Gyöngyösi, A. Bánvölgyi, A. Keszeg, S. Kárpáti, and N. M. Wikonkál, "In vivo assessment of potential carcinogenicity of multi-photon microscopy as the function of wavelength in the near-infrared range," J. Invest. Dermatol. **134**, S86 (2014).
14. D. Haluszka, K. Lőrincz, G. Molnár, G. Tamás, A. Kolonics, R. Szipőcs, S. Kárpáti, and N. M. Wikonkál, "In vivo second-harmonic generation and ex vivo coherent anti-Stokes Raman scattering microscopy to study the effect of obesity to fibroblast cell function using an Yb-fiber laser-based CARS extension unit," Microsc. Res. Tech. **78**(9), 823–830 (2015).
15. A. Kolonics, Z. Csiszovszki, E. R. Tőke, O. Lőrincz, D. Haluszka, and R. Szipőcs, "In vivo study of targeted nanomedicine delivery into Langerhans cells by multiphoton laser scanning microscopy," Exp. Dermatol. **23**(8), 596–605 (2014).
16. A. Komarov, H. Leblond, and F. Sanchez, "Theoretical analysis of the operating regime of a passively-mode-locked fiber laser through nonlinear polarization rotation," Phys. Rev. A **72**(6), 063811 (2005).
17. L. Huang, A. K. Mills, Y. Zhao, D. J. Jones, and S. Tang, "Miniature fiber-optic multiphoton microscopy system using frequency-doubled femtosecond Er-doped fiber laser," Biomed. Opt. Express **7**(5), 1948–1956 (2016).
18. Z. Várallyay and R. Szipőcs, "Stored energy, transmission group delay and mode field distortion in optical fibers," IEEE J. Sel. Top. Quantum Electron. **20**, 0904206 (2014).
19. H. Bao, J. Allen, R. Pattie, R. Vance, and M. Gu, "Fast handheld two-photon fluorescence microendoscope with a 475 microm x 475 microm field of view for in vivo imaging," Opt. Lett. **33**(12), 1333–1335 (2008).
20. D. M. Huland, Ch. M. Brown, D. G. Ouzounov, I. Pavlova, D. R. Rivera, W. W. Webb, and Ch. Xu, "Compact and portable *in vivo* multiphoton GRIN endoscope," in *Biomedical Optics and Digital Holography and Three-Dimensional Imaging Conference*, OSA Technical Digest Series (Optical Society of America, 2012), paper BTu3A.42.
21. B. A. Flusberg, J. C. Jung, E. D. Cocker, E. P. Anderson, and M. J. Schnitzer, "In vivo brain imaging using a portable 3.9 gram two-photon fluorescence microendoscope," Opt. Lett. **30**(17), 2272–2274 (2005).

1. Introduction

Nonlinear microscopy, such as two-photon excitation fluorescence microscopy (2PEF) and second-harmonic generation (SHG) microscopy is increasingly used to perform *in vivo* studies in life sciences, for example in dermatology [1–5]. These techniques enable us to investigate the morphology and monitor the physiological processes in the skin by the use of femtosecond pulse lasers (such as a broadly tunable Ti-sapphire laser [6]) operating in the near-infrared spectral range (680-1060 nm). Recent years brought revolutionary progress in the development of femtosecond pulse, all-fiber laser oscillators [7,8] and amplifiers being suitable for nonlinear microscopy. Fiber lasers are of great interest not only because of their considerably lower prices but also because they can easily be combined with endoscopy [9]. This latter feature greatly increases the utility of nonlinear microscopy for pre-clinical applications and tissue imaging.

There are a few commercial 3D microscope systems presently used for diagnostic purpouses in dermatology. Lucid's *VivaScope* is a confocal, handheld 3D mircoscope system that utilizes a cw near infrared laser for imaging through a pinhole for optical sectioning [10]. Due to the low photon energy and the low intensitiy of cw laser radiation applied, it is not suitable for single photon excitation fluorescence (1PEF) or nonlinear imaging (2PEF, SHG). Therefore, it does not offer chemical selectivity for the different tissue components. JenLab's *DermaInspect* system [1–5] has the advantage of utilizing nonlinear imaging techniques (2PEF, SHG, CARS) for microscopic 3D tissue imaging, however, the extra price that a customer (i.e. a dermatologist) has to pay for chemical selectivity is very high: it is basically the price of a femtosecond pulse tunable Ti:sapphire laser applied.

A few years ago we reported on the first broadly tunable, long-cavity Ti:sapphire laser oscillator [11] mode-locked in the net negative intra-cavity dispersion regime by Kerr-lens mode-locking. That laser delivered $\tau < 300$ fs pulses at 22 MHz repetition rate. Comparing

Biomedical Optics EXPRESS

the reported laser with a standard, 76 MHz Ti:sapphire oscillator (like the one used in Refs [1–5].) regarding two-photon excitation efficiency in a laser scanning microscope we see that the 22 MHz laser generates the same fluorescence signal at considerably, 1.82 times lower average power. This results in a reduced photo-thermal damage probability of biological samples. This fact along with the broad tunability and a low pump power requirement makes this cost-effective laser an ideal light source for nonlinear microscopy. In the same year, Baumgartl et al. reported on an all-fiber, two-wavelength laser source suitable for CARS microscopy, which laser delivered ~100 ps pulses at a few MHz repetition rate [12]. For high peak power of the (relatively long) laser pulses, which is crucial for nonlinear imaging, the repetition rate of the laser system was reduced by a programmable pulse picker, which was placed between the oscillator and the fiber amplifier unit operating at around 1030 nm. (Note that the nonlinear signal in a 2PEF or SHG imaging system scales inversely with the repetition rate as well as with the pulse duration of the laser as far as the average power is kept constant.)

Our aim was to considerably cut the price that a dermatologist has to pay for nonlinear microscopic imaging of the human skin. We also wanted to take the advantage of fiber optic delivery of the optical pulses to the (handheld) scanning microscope head. To achieve both our goals we decided to use highly efficient fiber lasers operating in the near infrared spectral range. The longer operation wavelength (compared to that of a Ti:sapphire laser) offers two main advantages: first, a lower scattering loss in the tissue, which allows deep tissue imaging without thermal damage of the skin; secondly, the longer wavelength (i.e. the lower photon energy) minimizes the risk of photochemical degradation (e.g., CPD formation) of the sample. This latter fact is extremely important from the point of view of human diagnostic applications, since in present 3D nonlinear microscope systems (e.g., in *DermaInspect*) Ti:sapphire lasers operating at 750 nm (for NADH excitation) and at 800 nm (for collagen detection) are used. In these imaging systems, the typical laser irradiation (average power) is at around 50 mW, which value is measured directly above the skin. According to our recent measurements [13], this power level has the risk of CPD formation in the DNA (at 750 nm excitation wavelength) when using typical pixel dwell time values of 5 μsec and a water immersion objective with a numerical aperture of NA = 1.0 in a scanning nonlinear microscope.

In the followings, we introduce our novel, handheld nonlinear microscope system comprising a ~2 MHz repetition rate Yb-fiber laser as a pulsed light source for nonlinear imaging. The system has the main advantages of the lower price of the fs laser applied, fiber optics flexibility, a relatively small, light-weight scanning and detection head, and a very low risk of thermal or photochemical damage of the skin. In order to mention some possible applications in dermatology, we show that our novel microscope system is capable of high quality, *in vivo* SHG imaging of the collagen content of murine skin at average power levels as low as ~5 mW. Among others, using SHG imaging of the collagen, one can investigate basal cell carcinoma [3] or follow the effects of obesity on dermal collagen alterations [14] for instance. For demonstration purposes in cosmetology and nanomedicine, we also used our two-channel 2PEF/SHG imaging system for *in vivo* visualization and for monitoring the uptake of Alexa Fluor 546 labelled nanomedicine by Langerhans cells [15] for a few hours.

2. Experimental setup

The block scheme of our *in vivo* nonlinear microscope imaging system is shown in Fig. 1. The primary pulsed laser source is an all-fiber, all-normal dispersion ytterbium ring oscillator (*FiberSource*, product of R&D Ultrafast Lasers Ltd, Budapest, Hungary) [8]. It operates at a ~36.4 MHz repetition rate and delivers (positively chirped) 10-12 ps optical pulses at λ_0 ~1030 nm with spectral bandwidths in the $\Delta\lambda$ ~8-12 nm range. The average power of the oscillator is P_{ml} ~10 mW. The repetition rate of the laser system is reduced by a fiber integrated, programmable pulse picker unit with controller electronics (product of *JenOptik*,

Biomedical Optics EXPRESS

Jena, Germany). The pulse picker is followed by a two-stage Yb-fiber amplifier (*FemtoCARS Stokes Unit*, product of R&D Ultrafast Lasers Ltd, Budapest, Hungary), which amplifies the rarefied optical pulses to an average power of ~200 mW. For our measurements, we typically set the repetiton rate of the amplified laser system in the 1 to 2 MHz range, which assures the highest peak powers without observable nonlinear distortion of the amplified pulses in the optical fiber amplifier. The low repetition rate, picosecond pulse Yb-fiber laser system has a FC/APC connector at the fiber output, which is introduced to an FC/APC fiber collimator (F220APC-1064, beam diameter: ~2.4 mm, product of Thorlabs Inc., USA) mechanically fixed in the imaging unit. Photos of the 2 MHz Yb-fiber laser system and the 2PEF/SHG imaging system (with plastic housing) are shown in Fig. 2.

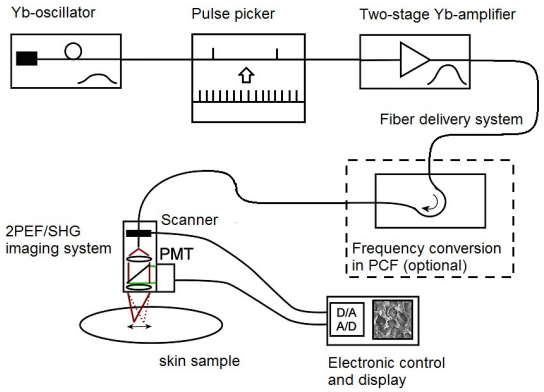

Fig. 1. Bloch scheme of the handheld 2PEF/SHG microscope imaging system comprising a 2 MHz mode-locked Yb-fiber laser.

Before entering the scanning head of our handheld microscope, the collimated laser beam passes through a small size transmission grating pair compressor, which reduces the pulse duration below 0.5 ps. The compressor unit, which includes a few mirrors and the grating pair, is fixed to the mechanical chassis of the imaging unit. Without any mechanical translation in the compressor unit (i.e. keeping the grating separation at a constant value), we can electronically control (practically minimize) the pulse duration of the compressed pulses, hence obtain the highest signal to noise ratio at a certain average power level. In the followings, we discuss in detail how our mode-locked Yb-laser oscillator can be characterized and electronically controlled for stable, Q-switching free operation. This is a basic requirement for safe operation of the *in vivo* imaging apparatus as well as for reliable operation of the pulse picker in front of our two-stage ytterbium amplifier.

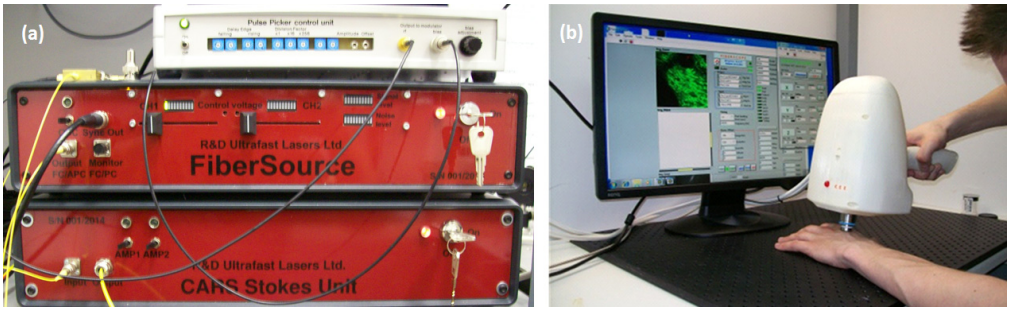

Fig. 2. (a) Photo of the 2 MHz Yb-fiber laser system comprising an AND type Yb-oscillator (*FiberSource*), a Pulse Picker (on the top) and a 2-stage Yb-fiber amplifier (*CARS Stokes Unit*). (b) Photo of the 2PEF/SHG imaging system with plastic housing and the control software interface. The plastic vacuum skin fixing unit including a 0.17 mm thick cover glass is removed in order to show the position of the microscope objective.

Biomedical Optics EXPRESS

2.1 The all-fiber, all-normal dispersion Yb-fiber ring oscillator

Passively mode-locked fiber lasers have gained scientific interest because of their potentially compact, environmentally stable and alignment-free design. Mode-locked operation of an Yb-fiber laser operating at around 1 micron can be obtained either in the net positive or negative dispersion regime. The former solution typically results in a more compact cavity design, since there is no need for intra-cavity dispersion compensating elements such as a grating pair, a prism pair, a hollow-core photonic crystal fiber, a higher-order mode fiber or a chirped fiber grating. Stable, cw mode-locked operation of an all-fiber, all-normal-dispersion ring laser, however, requires spectral filtering of the pulses. In [7], it was obtained by a fiber-integrated spectral filter having a spectral bandwidth of ~15 nm. A few years ago, we reported on an all-fiber, all-normal dispersion ring oscillator where pulse-shaping was based on nonlinear polarization rotation in the fiber together with spectral and temporal filtering by a fiber integrated polarizing element [8]. In that experiment, fiber-polarization controllers were used, in which the different paddles were manually set for optimum cw mode-locked operation of the laser.

In the followings, we describe our similar all-fiber, all-normal-dispersion Yb ring oscillator, in which the polarization controller element is replaced by an electronically controllable device. This simple upgrade in the laser setup, together with some improvement in the laser control electronics and data analysis hardware and software, allowed us to perform a detailed analysis on the mode-locked laser performance as the function of different polarization states of the optical pulses reaching the fiber integrated polarization element. Based on such an analysis, one can precisely control the mode-locked operation of an all-fiber, all-normal dispersion Yb-fiber ring laser.

The Yb-fiber ring laser setup is shown in Fig. 3. A highly doped ytterbium fiber (Yb) is used as the gain media, which is pumped by a 976 nm laser diode (LD) via a 980/1030 nm wavelength-division multiplexer (WDM). The Yb-doped fiber is followed by an isolator (ISO) realizing the unidirectional cavity. The initiation and stabilization of mode-locking is obtained by a semiconductor saturable absorber (SA). Between the SA and the polarizing beam splitter (PBS), we placed the electronically adjustable polarization controller (PC, Type: PolaRITE III - Mini dynamic polarization controller, product of General Photonics). The rest of the components are the same that were reported in [8].

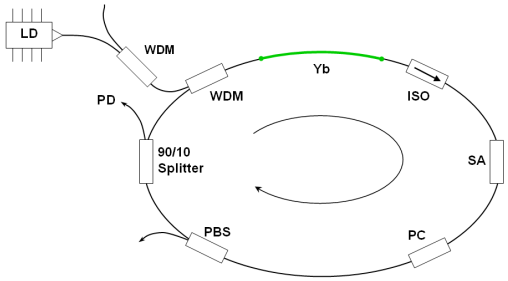

Fig. 3. Setup of our AND type Yb-fiber seed oscillator.

The nonlinear polarization evolution of the optical pulses results in a variation of the polarization state along the pulse spectrum, leading to a strong spectral filtering effect by the PBS [8]. The PBS is followed by a 90%-10% splitter, where the 10% output port is directed to a fast photodiode (PD, Type: DET10C/M, product of Thorlabs). The laser output detected by the fast photodiode (PD) is analysed by a radio-frequency spectrum analyser (FSV3, product of Rohde&Schwarz). Depending on the contol voltage values of the polarization controller (PC), we can obtain cw mode-locked, Q-switched or noise-like pulses, as shown in Fig. 4. In the figure, the radio-frequency spectrum (horizontal axis) is measured over a +/– 1 MHz bandwidth around the laser central frequency of 36.4 MHz.

Biomedical Optics EXPRESS

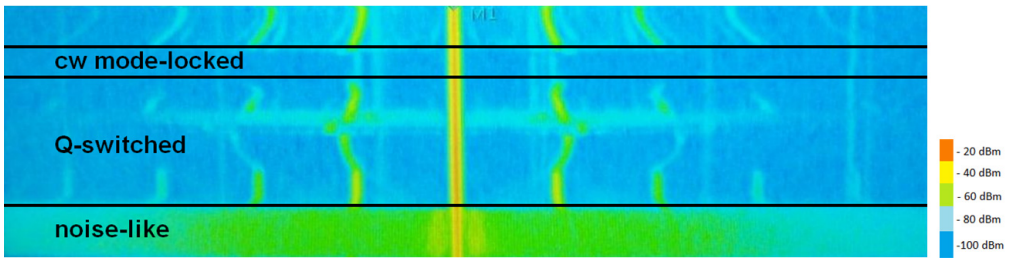

Fig. 4. Measured radio-frequency power spectra at different control voltages (vertical axis) at around the central frequency of the all-fiber, all-normal-dispersion Yb-fiber ring laser. Central frequency: 36.4 MHz, frequency span: 2 MHz.

Unfortunately, the radio-frequency spectra measured by the spectrum analyser could not be directly used for the optimiziation of the cw mode-locked performance of the laser by setting the contol voltages of the polarization controller by a computer or a microcontroller. In order to solve this problem, we developed high sensitivity, radio-frequency amplifiers and filters providing electronic signals proportional to the measured signal power (P_{signal}) and the measured single sideband noise power (P_{noise}). Taking the advantage of this new electronics, we could easily measure P_{signal} and P_{noise} as the function of the control voltages applied on the polarization controller device, as shown in Fig. 5. Please note that this function is periodic for both the Quarter-Wave Plate Control Voltage (horizontal axis) and the Half-Wave Plate Control Voltage (vertical axis), and only one period is displayed in Fig. 5.

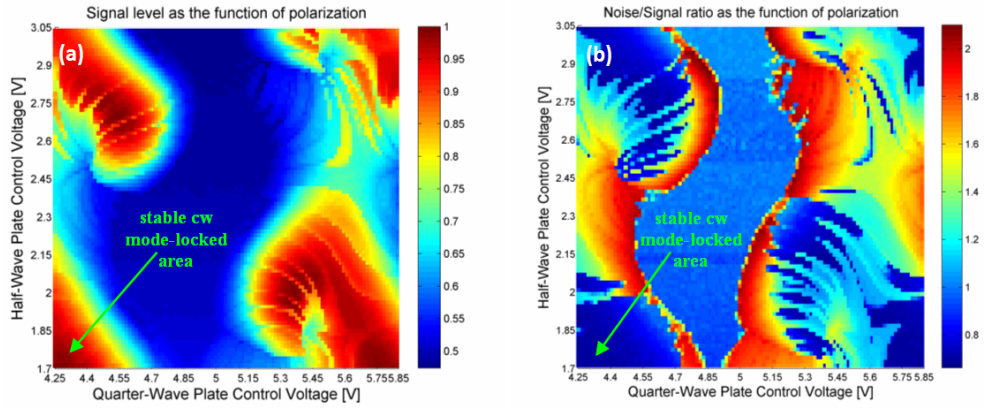

Fig. 5. (a) Measured signal power and (b) normalized noise power as the function of control voltage on the polarization controllers.

For the stable cw mode-locked operation of the Yb-fiber laser, we require high signal levels (high P_{signal} values) and low rms noise (low P_{noise} values). This requirement can be easily visualized if we plot the normalized noise power (P_{noise} /P_{signal}) as the function of control voltage values (see Fig. 5, right). The stable cw mode-locked operation area is indicated by a dark blue color in the figure. During the experiments with our new laser setup and electronics, we had several interesting findings, which are summarized as follows: first of all, the shape of the "stability maps" that are shown in Fig. 5 were significantly different depending on the pump power, length of the SM fiber in front of the PBS, the round-trip time of the laser and other parameters, such as the method of rolling up of the fiber onto the holder mechanics. Without going into details, it is important to note that large stable cw-mode locked areas could be obtained only if we rolled up the optical fiber in a figure-8 configuration and provided sufficiently high pump power for the Yb-oscillator. In order to come to a stable laser configuration, like the one demonstrated in Fig. 5, we preferred to take several "stability maps" during the different stages of the mechanical fixing of the optical

Biomedical Optics EXPRESS

fibers and components, and correct the configuration accordingly. Having the laser configuration fixed and the final "stability maps" recorded, we could easily find the optimum control voltage values of the polarization controller, for which the laser operated in the cw mode-locked regime at the highest average signal and the lowest noise power levels (shown in Fig. 5 by arrows).

There are two additional issues that should be mentioned before using the method introduced for computer or microcontroller control of an all-fiber, all-normal dispersion Yb-fiber ring oscillator for everyday use. Firstly, the Yb-fiber laser tested (and the corresponding stability map) had some thermal drift according to the temperature change in the laboratory, even if all of the optical components and fibers were fixed in the housing. This is due to the temperature dependent, mechanical stress induced birefringence in the SM fiber components. When using such components, this fact requires a continuous, fine re-adjustment of the polarization control voltages during the operation of the laser in order to keep the highest signal to noise ratios. This unfavourable effect, however, can be minimized by applying PM fiber optic components where applicable. Secondly, the all-fiber, all-normal dispersion Yb-fiber ring oscillator reported here had some inherent nonlinearity, which resulted in an optically bistable behaviour [16], as demonstrated in Fig. 6. For recording the „stability maps" shown in Fig. 6, the quarter-wave plate control voltage values (horizontal axis) were increased and reduced for the even and odd rows, respectively. It is clearly seen that the cw mode-locked status of the laser had a feedback to the stability maps (the stable/unstable borders were slightly shifted), which fact arouses additional challenges when writing a computer code for laser control.

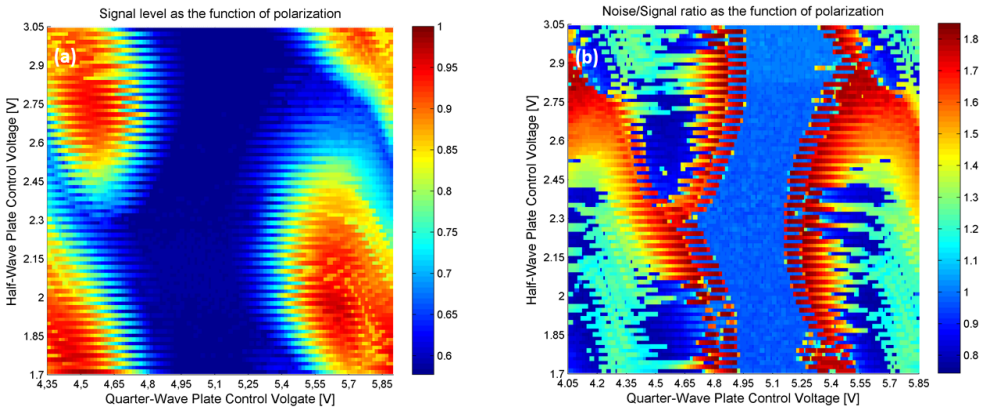

Fig. 6. Demonstration of optical bistability of the all-fiber, all-normal dispersion Yb-fiber ring oscillator. Parameters are the same than in Fig. 5, but the data plotted were recorded for increasing and reducing quarter-wave plate control voltages for even and odd rows, respectively.

Regarding the tuning range of the fiber laser system we can say that the Yb-oscillator can be tuned from 1025 nm to 1042 nm by the use of the polarization controller, which might limit the application of the current laser setup compared to that of utilizing Ti:sapphire lasers. However, fiber laser technology can offer a solution to this problem: properly designed, highly nonlinear photonic crystal fibers can convert light from one wavelength to another one by nonlinear processes such as fiber optical parametric frequency conversion [12]. To this end we have made some numerical simulations and preliminary experiments using our current laser parameters. We found that our 2 MHz, ~1030 nm laser output can be converted to shorter wavelengths depending on dispersion parameters of the photonic crystal fiber. The efficiency of this nonlinear frequency conversion process is at around 5%, higher conversion rates at around 10% could be obtained only at the expense of lower pulse quality. At the moment, the average power of the frequency converted laser output is too low for nonlinear

Biomedical Optics EXPRESS

imaging. However, it can be improved by increasing the average power of our Yb-amplifier, i.e. by building an additional amplifier stage. Work is in progress (see Fig. 1, frequency conversion in PCF) to build an all fiber laser system suitable for CARS microscopy [12] and exciting different fluorophores such as NADH or eGFP at around ~780 nm and ~900 nm. An alternative solution to extend the operation range of fiber lasers into the red is frequency-doubling of a femtosecond Er-doped fiber laser [17] for instance, but the low temporal quality of the laser pulses reported in Ref. 17 arouses laser safety concerns in this latter case. In both cases, dispersive properties of optical fibers [18] play an important role and can improve laser performance.

2.2 The pulse picker and the two-stage Yb amplifier

The fiber integrated, programmable pulse picker unit with controller electronics requires TTL level synchronization input signals, which can be easily generated from the electronic signal of the fast photodetector (PD) by using some home built comparator electronics. The two-stage Yb-amplifier is pumped by wavelength stabilized 976 nm laser diodes similar to those used to build the Yb-oscillator with cw output powers up to 500 mW. For seeding the first amplifier stage, we used the polarized PBS output of our oscillator. Pump powers of the laser diodes and lengths of the Yb-doped fibers were optimized for the ~1.89 MHz repetition rate of the seed pulses, since the ~10 mW average output power of the Yb-oscillator operating at 36.4 MHz was reduced by a factor ~20 by the pulse picker. After this optimization process, the two-stage Yb-amplifier delivered ~15 ps long optical pulses at around 1030 nm at ~1.89 MHz repetition rate with an average power of ~200 mW without observable ASE content. The positively chirped output pulses were compressed by a transmission grating compressor with grating separation of ~80 mm resulting in sub-500 fs long, ~50 nJ pulses for nonlinear imaging.

2.3 The imaging setup

During the last couples of years, there have been several attempts aiming for the development of a fiber laser based or fiber delivered nonlinear microendoscope systems [17, 19–21]. As the operation laser wavelength reaches that of the Yb-fiber lasers at around 1 μm, the risk of photochemical damage due to CPD formation in the DNA is negligible [13]. That is why the main possible source of sample damage due to laser irradiation is of thermal origin in *ex vivo* or *in vivo* biological measurements. In order to minimize the thermal load on the sample, there are a few requirements that we list below. First of all, the operation wavelength of the pulsed laser source should be close to the 2P excitation fluorescence maximum of the fluorescent labelling applied or that of the autofluorescence of the biological sample. In order to meet this requirement, we have developed an optical fiber based wavelength conversion unit similar to the one published in Ref. 12 (see also the dashed box in Fig. 1), however, the power we have obtained so far was too low for nonlinear imaging. Therefore, a detailed discussion of this optical fiber based wavelength conversion unit is not provided in this paper. Secondly, the laser should deliver the highest peak powers at the lowest average power for the highest signal to noise ratio. To this end, one can use shorter and shorter laser pulses at the expense of higher sensitivity for temporal and spatial dispersive effects. This latter one is an enormous problem in microendoscope systems utilizing GRIN lenses for focusing the laser beam, since a GRIN lens itself is not compendsated for chromatic aberrations. Furthermore, a GRIN lens has a limited numerical aperture, which ultimately determines not only the focal spot size and hence the resolution of the microscope, but also the maximum focused intensity of the laser pulses applied and the signal level that can be reached at a certain average power level and pulse duration. From this respect, the best choice is a high numerical aperture, IR corrected microscope objective that focuses a well shaped laser beam onto the sample. The third factor that determines the thermal load of the biological sample is the scanning method applied. For nonlinear microendoscope systems, there are a few possible fiber scanning

Biomedical Optics EXPRESS

techniques that have been demonstrated: piezo scanning of the fiber ends in a spiral or a Lissajous curve. In the first case, the thermal load on the sample is the highest at the middle of the imaged area, which limits the maximum average power level that can be applied without thermal damage of the sample. In the latter case, the thermal load on the biological sample is nearly uniform over the investigated area. However, data collection and imaging is rather difficult and requires a difficult calibration process at different imaging speeds and areas. One can also apply MEMS [17] for beam steering, but the laser beam size and the field of view is typically limited.

According to the design issues listed above and discussed in Ref. 11 in details for minimum thermal load on the biological samples, our handheld scanning 2PEF/SHG imaging head comprises an x-y galvano scanner unit designed for laser beams of ~2.3 mm in diameter (Cambridge Technologies), and a 1:3 telescope system custom designed for an *EC Plan-Neofluar 40x/0.75* objective (Carl Zeiss, Germany). This objective is optimized for a cover glass having a physical thickness of 0.17 mm. The use of (a replaceable) cover glass in our imaging system assures in longer term that the skin of each patient can be investigated by a medical device that does not carry any infection from previous patients. Additionally, skin position can be fixed to the cover glass by a properly designed vacuum system that should be necessary for high resolution, 3D pathological measurements, which takes a few minutes even at a 200 kHz sampling rate.

The physical length of the whole microscope imaging system is at around ~180 mm, which includes both the scanner unit and the microscope objective. The real challange in designing such a scanning microscope system was the design of the 1:3 imaging telescope between the scanner mirrors and the microscope objective by the use of commercially available lenses. For this work, we applied an optical design software (Zemax release 13 SP 2 Standard (64bit); Zemax LLC, Redmond WA, USA). The final design of the telescope system is illustrated in Fig. 7, where a screenshot from the Zemax program is displayed. On the left, the rays start from the scanner mirrors (more precisely, from the half way position betwen the x and y scanner mirrors). The initial beam diameter is 3 mm. On the right, the beams reach the entrance aperture of the microscope objective having a diameter of 8.9 mm. The physical distance between the scanner plane and the entrance aperture is 135 mm, while the microscope objective itself is 42 mm long.

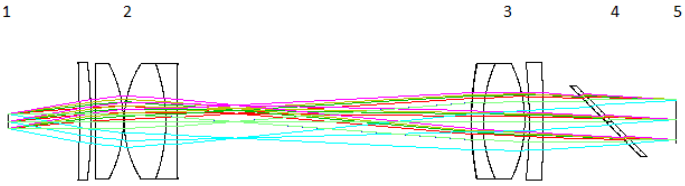

Fig. 7. Optical design of the achromatic 1:3 imaging telescope (comprising two lens groups (2 and 3) between the scanner mirrors (1) and the entrance aperture of the microscope objective (5). A dichroic beamsplitter (4) is placed in front of the microscope objective.

Biomedical Optics EXPRESS

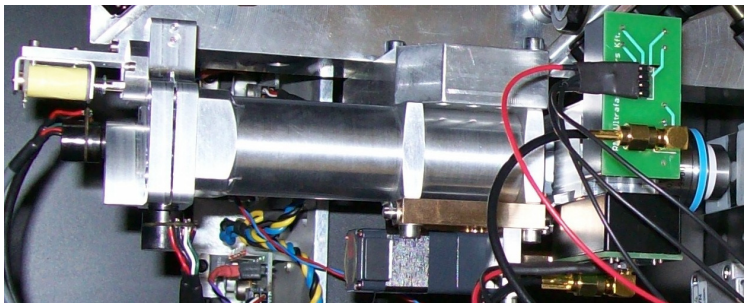

Fig. 8. Photo of the laser scanning 2PEF/SHG imaging system. The optical elements shown in the optical design (see Fig. 7) are fixed within the metallic tube between the two scanner mirrors (left) and the microscope objective (right).

In Fig. 8, a photo of the laser scanning 2PEF/SHG imaging system is shown. The 2PEF/SHG signal is detected by two small size PMT detectors (Hamamatsu, Japan) supplied with properly chosen dichroic and bandpass filters. The analogous electronic signals of the PMT detectors are amplified and digitized by some home-built electronics.

3. Imaging results

We tested the handheld nonlinear microscope imaging system for different *in vitro and vivo* murine skin samples. For our 2PEF and SHG *in vivo* measurements, first we optimized the repetition rate of our laser system for the highest nonlinear signal before reaching the low frequency limit of any thermal or photochemical damage of the skin samples. Then, we used the optimized setup for (one channel) collagen measurement of *in vivo* murine skin samples. Finally, we used a two-channel setup for *in vivo* monitoring of penetration of fluorescent labelled nanomedicine into the skin for a few hours.

3.1 Signal dependence on repetition rate of the laser system

We summarize the results of our laser frequency dependent imaging measurements in Fig. 9, where SHG images of dermal collagen in an *in vitro* murine sample are shown that were recorded at different pulse repetition rates. For recording the SHG images, the pulse picker performance was optimized at each frequency without adjusting the grating pair compressor or the polarization controller settings. In theory, the second-order nonlinear signal (2PEF or SHG) amplitude would scale inversely with the repetition rate of the laser system if the average power and the pulse duration are kept constant. In practice, however, we could not measure such an exact dependence due to the imperfect settings of the pulse picker and/or some nonlinear effects in the two-stage Yb-amplifier -even when the pulse spectrum of the oscillator was kept constant. In spite of these uncertainties, we dare say that the tendency is clear: the lower the repetition rate of the Yb-laser amplifier the higher the measured SHG signal. For our laser system, we found an optimum performance at around 1.89 MHz (when the pulse separation is ~0.53 μs), which is well below the thermal time constant of living tissues (i.e., water, see Ref. 11 and references therein), which is at around 1 μs, hence we do not have accumulated thermal effects in our biological samples. Note that at laser repetition rates below the thermal constant mentioned, i.e. below 1 MHz, not the average laser power but the energy of a single laser pulse determines the local temperature increase in the focal point of the laser beam at fixed pixel dwell time values.

Biomedical Optics EXPRESS

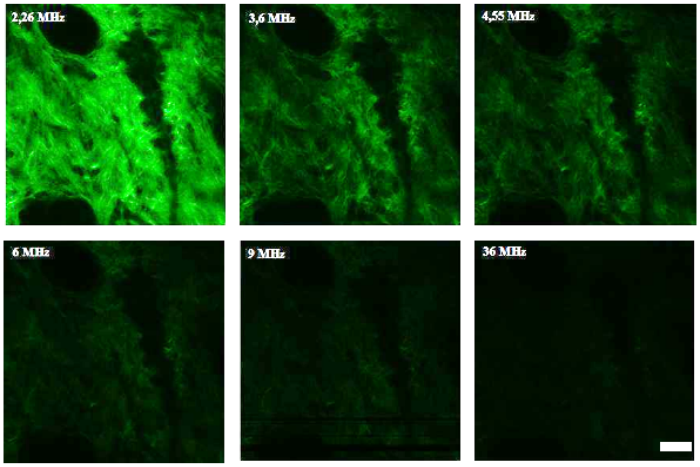

Fig. 9. SHG signal intensity as the function of repetition rate of the Yb-fiber laser. Average power: 5 mW (measured after the microscope objective). Pixel dwell time: 5 µs. Operation wavelength: 1030 nm. Fixed transmission grating distance of ~80 mm. Ex-vivo murine skin sample. Scale bar: 20 µm.

3.2 Collagen measurement by SHG imaging

After optimizing our laser and imaging setup described above, we have performed a high number of *in vivo* SHG imaging measurements on the collagen content of living murine skin samples. Having *in vivo* human applications in mind, using this visual information a dermatologist can investigate tumor borders (e.g., in case of basal cell carcinoma [3]) or to follow biochemical processes in the human skin, such as the effects of obesity on dermal collagen alterations for instance [14]. SHG image of the collagen distribution in a murine skin shown in Fig. 10 was recorded at ~5 mW average power. The pixel dwell time was set to 5 µs, which corresponds to our 200 kHz sampling rate. The raw digital images taken by the handheld microscope system were postprocessed by the *ZEN 2011* image processing software of Carl Zeiss.

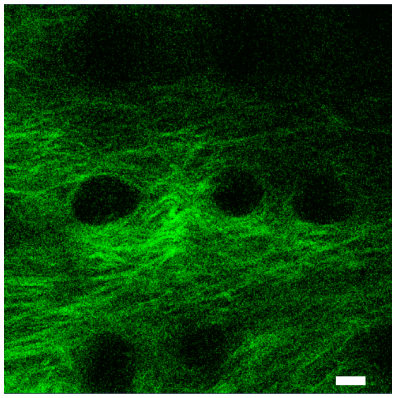

Fig. 10. *In vivo* SHG image of collagen in a murine skin sample being measured by the use of an Yb-fiber laser operating at a 1.89 MHz repetition rate. The laser average power measured directly above the skin is 5 mW. Scale bar: 20 µm.

3.3 Monitoring the penetration of nanomedicine into the skin in vivo

Epidermal Langerhans cells (LCs) function as professional antigen-presenting cells of the skin. In a recent experiment [15] we investigated the LC-targeting properties of a special mannose–moiety-coated pathogen-like synthetic nanomedicine DermaVir (DV), which is

Biomedical Optics EXPRESS

capable to express antigens to induce immune responses and kill HIV-infected cells. In order to visualize the uptake of Alexa-labelled DV (AF546-DV) by LCs *in vivo*, we used a commercial LSM 7MP scanning 2PEF microscope system of Carl Zeiss. Knock-in mice expressing enhanced green fluorescent protein (eGFP) under the control of the langerin gene (CD207) were used to visualize LCs. The (Ti:sapphire) operation wavelength was set to 890 nm for efficient excitation of both the eGFP and the AF546 dye. During our studies we found that after 1 hour AF546-DV penetrated the epidermis and entered into the eGFP-LCs.

In order to test both imaging channels ("green": 500-550 nm, "red": 565-610 nm) of our handheld device, we repeated this measurement, the result of which is shown in Fig. 11. We can observe that the Langerhans cells, which are a part of the immune system, accumulate the AF546-labelled nanoparticles after 1 hour of the topical treatment by nanomedicine of the skin. Due to the very low risk of thermal or photochemical damage of the skin samples, we consider our device as a safe, cost efficient, potential candidate for similar clinical applications in dermatology, cosmetology or nanomedicine research.

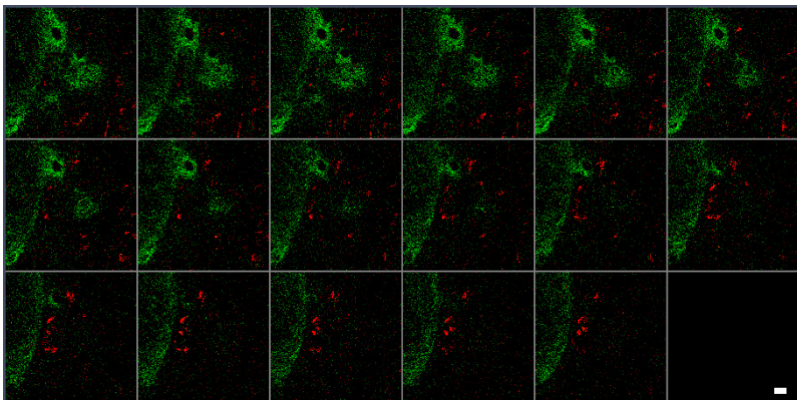

Fig. 11. *In vivo* penetration measurement of Alexa-546 labelled nanoparticles (AF546-DV) in murine skin. Excitation wavelength: ~1030 nm, z-stack image (128x128 pixels/frame). Green: SHG signal of collagen. Red: fluorescence signal of AF546-labelled nanoparticles 1 hour after of the topical treatment by nanomedicine of the skin. One can observe that the Langerhans cells, which are a part of the immune system, accumulate the AF546-labelled nanoparticles [15]. Scale bar: 50 μm.

5. Summary

A novel, Yb-fiber laser based, handheld 2PEF/SHG microscope imaging system has been introduced. We demonstrated that the system is suitable for *in vivo* imaging of murine skin at an average power level as low as 5 mW at 200 kHz sampling rate. It has the main advantages of the low price of the fs laser applied, fiber optics flexibility, a relatively small, light-weight scanning and detection head, and a very low risk of thermal or photochemical damage of the skin. Owing to the advantageous features described, we regard it as a new useful diagnostic or imaging tool for clinical applications in dermatology or cosmetology.

Funding

This research was supported by the Hungarian Development Agency (NFÜ) under contract TECH-09-A2-2009-0134 and by R&D Ultrafast Lasers Ltd.